2007 Urban Remote Sensing Joint Event

Model Based Building Recognition from Multi-Aspect InSAR Data in Urban Areas

A. Thiele, E. Cadario, K. Schulz, U. Thoennessen
FGAN-FOM
Research Institute for Optronics and Pattern Recognition
Ettlingen, Germany

U. Soergel
University of Hannover
Institute of Photogrammetry and GeoInformation
Hannover, Germany

Abstract— **The achievable ground resolution of state-of-the-art synthetic aperture radar (SAR) sensors enables the analysis of urban areas with industrial as well as residential character. In this paper, an approach is proposed to detect and reconstruct small as well as extended buildings from multi-aspect high resolution InSAR data sets. The recognition of buildings is supported by knowledge based analysis considering SAR-specific effects such as layover, radar shadow and multipath signal propagation. But especially in dense built up areas those effects can also lead to a reduction of the reconstruction quality e.g. in the case of adjacent trees or other buildings. In those cases the results can be significantly improved by a combined analysis of multi-aspect data. The presented approach exploits amplitude, phase, coherence data and classification results. That is demonstrated in an urban environment for an InSAR data set, which has a spatial resolution of about 30 cm and was taken from two orthogonal flight directions.**

I. INTRODUCTION

In the last decades Synthetic Aperture Radar (SAR) has become a key remote sensing technique. The main reasons are its independence from the time of day and all weather capability. High Resolution SAR-data with metric resolution allow the exploitation of such data for the analysis of urban areas. The recognition of buildings e.g. has been studied for city cores with high buildings [1], rural areas [2], and industrial plants [3], [4]. Today, modern experimental sensors achieve geometric resolution of amplitude data in the decimeter scale [5]. In such data many additional building features become visible, that are useful for analysis [6], [7] and even smaller units like residential buildings can be detected. Beside amplitude images, also interferometric phase and coherence can deliver additional information for building detection and reconstruction and the frequently observable problem of occluded areas in SAR images especially in dense urban areas can be significantly reduced by using information from different aspects [8]. In recently published work, urban DSM extraction from one high resolution interferometric SAR pair by feature fusion was proposed [9] considering also amplitude, coherence and interferogram.

In this paper, a model-based approach for detection and reconstruction of small buildings like multi family houses up to larger buildings such as industrial halls from multi-aspect high resolution InSAR data is proposed. Primitives are segmented independently in the magnitude images of two orthogonal aspects in slant geometry and afterwards projected into the world coordinate system. In the set of fused primitives building hypotheses are derived and final candidates are filtered according to features calculated from the amplitude, interferometric phase, and coherence data. An additional filter criterion is derived from a rule based classification taking into account the amplitude and coherence data. For this purpose the commercial software tool Definiens Professional from Definiens AG is used for segmentation and classification of the test site. Meanwhile this software was successfully used for several tasks in the classification of SAR imagery [10], [11]. The information that in the considered urban area hints exist for vegetation like broad-leaved trees is quite helpful to supplement the reconstruction process.

This paper is organized as follows. The special illumination effects of SAR from different aspects in vicinity of buildings are shown in Section II. The model-based approach for the detection and reconstruction of different kinds of buildings from multi-aspect InSAR data is described in Section III. The results in comparison to ground truth data (cadastral footprints and LIDAR DSM) and the conclusion are presented in Section IV and V.

II. APPEARANCE OF BUILDINGS

In this section, the appearance of small and extended buildings in InSAR data is discussed. The focus is on typical building features observable in SAR data which are exploited in the presented approach.

A. Visualization of Effects by Simulation

The presented simulation is focused on the visualization of the impact of geometric features such as building size and orientation. Therefore Lambertian backscattering properties are assumed, the entire SAR processing incorporating object features such as roughness and dielectric constant are not considered [12]. The building models on top of Fig. 1 were simulated with the software SARView Light (EADS) for orthogonal flight directions [13]. The resulting magnitude images for a right looking sensor are shown in Fig. 1. For flight direction 1, layover and roof areas are distinguishable in the simulation result of both buildings. For flight direction 2, only the larger building has a visible roof area in the simulated SAR

image. Within the smaller building, the intensity area behind the brightest stripe could be interpreted wrongly as roof, but it results only from layover signal from lower parts of the building wall and ground.

B. Buildings in Real InSAR Data

For this study SLC InSAR imagery from Intermap Technologies [14] covering a part of the city of Dorsten, Germany, was analyzed. The InSAR data was taken from a single pass interferometric antenna configuration with a spatial resolution of about 38 cm in range and 16 cm in azimuth direction (X-Band). The effective baseline was approx. 2.4 m and the off-nadir angle θ increases from 28° to 52° over swath. The SAR data were taken twice from orthogonal viewing directions, i.e. from each direction two image pairs were recorded. The overlapping area covers five square kilometers of an urban area characterized by a mixture of residential and industrial buildings.

A small subset of the scene is shown in Fig. 2. It includes buildings of structure similar to the models used for the simulation (Fig. 1). The layover area and the backscatter signal of the dihedral corner reflectors are visible in the magnitude data. The roof area is hardly detectable even for the larger building in comparison to the simulation result. This is mainly caused by different roof material properties (often rather smooth surfaces, violating the Lambertian simulation model), by superstructures and by interaction effects between adjacent buildings and trees. The latter is also true for the shadow parts.

III. Building Detection and Reconstruction

Based on the conclusions from Section II, approaches as proposed in the literature [3], which model roof areas as regions of similar magnitude, fail for the high level of detail in the given data set. The approach proposed here is based on edges and lines, because in high resolution SAR data those are well detectable [7]. Also in [4] such building hints are used for the reconstruction of industrial buildings by sampling L- and T-structures. There a stereoscopic sequence of SAR images from one aspect was investigated.

The here presented approach is a combination of the proposed algorithms in [15] and [16], tailored for the detection and reconstruction of small respectively large buildings. The searched building model is restricted to a rectangular footprint and a flat roof. The reconstruction of small buildings uses sampled L-structures as building hints caused by double bounce reflection (corner line) and benefits from complementing information of orthogonal views. Due to the different views it is possible to compensate frequently occurring occlusions due to other buildings or trees, which often hamper building reconstruction from one aspect alone. In comparison the reconstruction of extended buildings exploits a set of typical SAR phenomena such as layover, corner line, roof signature, and shadow. A discrimination of all generated building candidates (small and extended buildings) is based on classification results and candidate features calculated from the InSAR heights.

A. Pre-Processing

1) Calculation of Magnitude Images: The pre-processing of the magnitude images includes speckle reduction accomplished with Gamma-Map filter [17]. The subsequent fusion of the four magnitude images (two antennas, two recording times) comprises a subpixel registration of the images based on coherence maximization. The fusion of the magnitude images is carried out using the maximum (*max*), minimum (*min*) or average (*avg*) operator. These images are the base for the segmentation step of primitives (lines and edges).

2) Calculation of Interferogram: The formation of the interferometric heights comprises also a subpixel registration. The subsequent interferogram generation includes a multi-look filtering and is followed by the steps of flat earth compensation, phase centering and phase correction. With the phase centering a phase distribution with zero mean can be

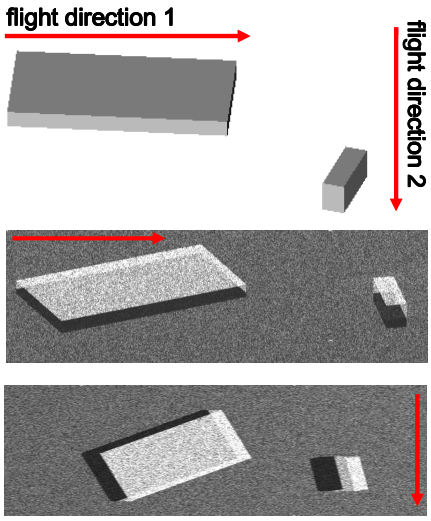

Figure 1. 3D model for simulation; simulated magnitude images of flight direction 1 and direction 2

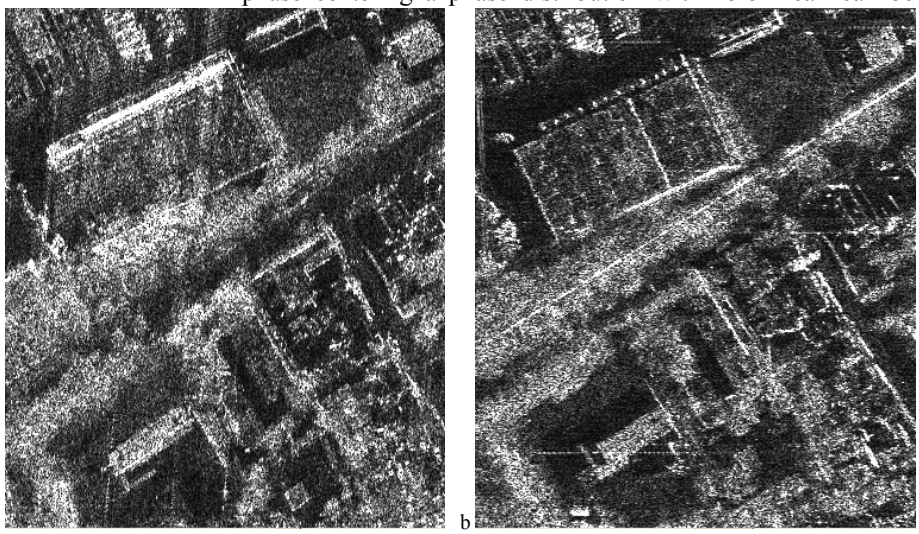

Figure 2. Part of original magnitude images of flight direction 1 (a) and direction 2 (b)

Figure 3. Part of interferometric height images of flight direction 1 (left) and direction 2 (right) in slant range geometry

achieved. The step of phase shifting is integrated in the conversion from phase differences into terrain heights. Phase values significantly below the local average are shifted upwards by 2π. This leads to a reduction of height discontinuities at building locations. The calculated height images are shown in Fig. 3. For the projection into the world coordinate system the InSAR heights in areas with poor coherence and high height standard deviation were smoothed. This was necessary to achieve good geocoding results and to avoid gaps in the target coordinate system.

3) Classification: The Definiens software is applied to classify the test site with an object oriented technique. Magnitude (Fig. 4a,e), coherence (Fig. 4b,f) and Coefficient of Variation (COV, Fig. 4c,g) are used as input layers for the segmentation and classification process. A basic rule system for classification is implemented that uses relationships between these three layers. In [18] relations between backscattering coefficient and interferometric coherence are denoted for several vegetation and different surface types. This knowledge is included in the rule system to discriminate *Vegetation* (broad-leaved trees), *Medium Rough Surfaces* and *Scatterer*. The class *Scatterer* is here defined as areas that show high magnitude, high coherence and high COV. Furthermore suitable membership functions are adapted for every class and input layer. The evaluation of the rules with the Definiens fuzzy classifier leads to the results depicted in Fig. 4d,h. This classification process is applied for both flight directions and the results are fused by intersection (Fig. 4i). Only those regions are considered that have the same class in both directions. The classification results are applied as initial information for discrimination of building hypotheses.

B. Assembly of Building Hypotheses

1) Segmentation of Primitives in the Magnitude Images: The segmentation of primitives based on the pre-processed magnitude images. Depending on the operator (*min, max, avg*), different features of the SAR signature can be better distinguished. The max-fused image is best suitable for the extraction of bright lines using the Steger-Operator [19]. The avg-fused image is equivalent to multi-look processing of four initial images and is useful for the extraction of side lines applying the Canny-Operator [20]. In the min-fused image clutter signals propagating into shadow areas vanish. In this image a segmentation step characterized by approximating the border of dark regions with lines, delivers edges at the near side of the region with respect to sensor position. For all

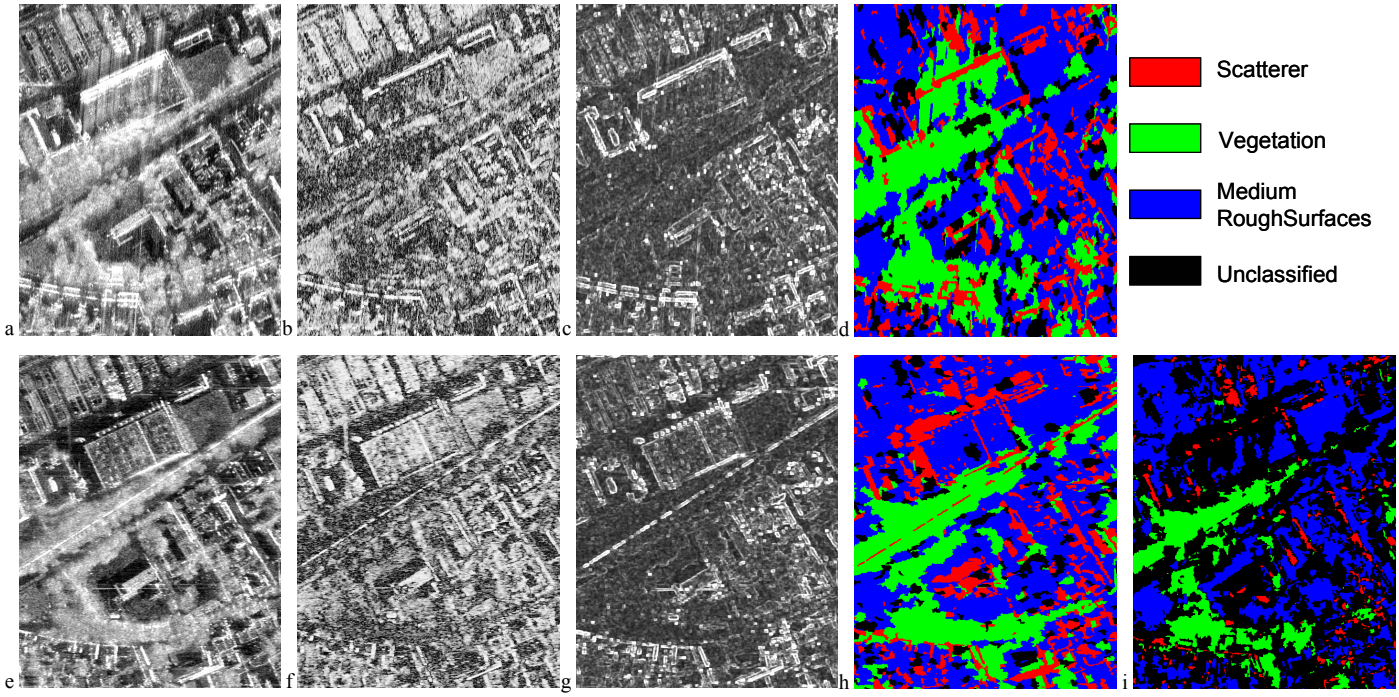

Figure 4. Magnitude (a, e), coherence (b, f) and COV (c, g) images as input data of classification step; Classification results of flight direction 1 (d) and direction 2 (h); Fused classification results (i)

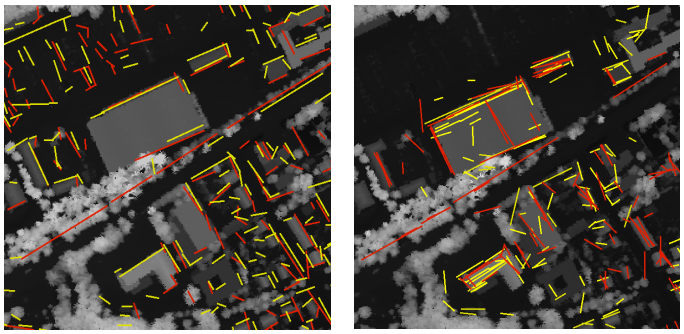

Figure 5. LIDAR DSM overlaid with projected primitives of flight direction 1 (yellow) and direction 2 (red) for small (left) and extended (right) building generation

extracted primitives (lines and edges) a set of mean values is calculated in their neighborhood regarding magnitude, coherence and height values. For the reconstruction of small buildings only lines caused by a dihedral corner reflector between ground and building walls are considered, because the other primitives are often not visible [15]. In the case of extended buildings all the primitives are used. The calculated feature values are used to distinguish between Sensor-Close, Sensor-Far, and Side primitives.

2) Fusion of Primitives: The resulting primitives of both flight directions are individually projected from slant range into ground range geometry in the world coordinate system. This projection is performed individually for each primitive using the calculated InSAR heights for every primitive in their surrounding area. In Fig. 5 the overlay of reference LIDAR DSM with the primitives of flight direction 1 (yellow) and direction 2 (red) is visualized to show the benefit of multi-aspect data exploitation. These sets of primitives are used for the subsequent building hypotheses generation.

3) Generation of Building Candidates: Starting with the generation of small building candidates the first step comprises the search of line pairs, which must meet angle, bridging and gap tolerances to be a L-structures. The union of primitives from both directions reveals the benefit of orthogonal views. Based on the given flight directions and the sensor orientation a filtering of the extracted L-structures is possible. On condition that the detected primitives are caused by a double bounce reflection between building wall and ground, only L-structures with suitable orientation are considered [15]. In the next step quadrangles (parallelograms) are derived from the final set of L-structures (Fig. 6a).

In the case of extended building reconstruction the generation step exploits all primitives. From the primitives set unions, quadrangles are assembled by a production system proposed in [17]. As a constraint at least one edge of the quadrangle facing one of the sensors must be derived from a line of bright scattering (Sensor-Close edge). Analogous, an object of the group Shadow edges is required at the Sensor-Far edge of the quadrangle. Optionally Side edges are also taken into account. The set of assembled quadrangles of the test site is shown in Fig. 6b.

4) Discrimination of Building Hypotheses: Only a subset of the generated parallelograms and quadrangles actually coincide with real buildings, furthermore many competing (overlapping) quadrangles are present. The first discrimination step exploits the fused classification results. The overlay of classification result and building candidates (Fig. 6c) shows intersection between hypotheses and the class *Vegetation* (dark gray). Using *Vegetation* fraction inside a building hypothesis as filter criterion, the hypotheses depicted in Fig. 6d are remained. The decision which members of this result are considered further on is based on the features derived from the related smoothed InSAR elevation data (mean height and standard deviation of height inside the hypotheses as well as size of hypotheses). The mean height value of the hypotheses has to be some meters above mean terrain height according to the local typical architecture and the height standard deviation has to be lower than a threshold. The subsequent assessment step of the remaining hypotheses valued size of building and height standard deviation of building, and if remaining quadrangles overlap best ratio between these features is taken. In the last step for each final building candidate the corresponding building footprint is determined by a minimum bounding rectangle.

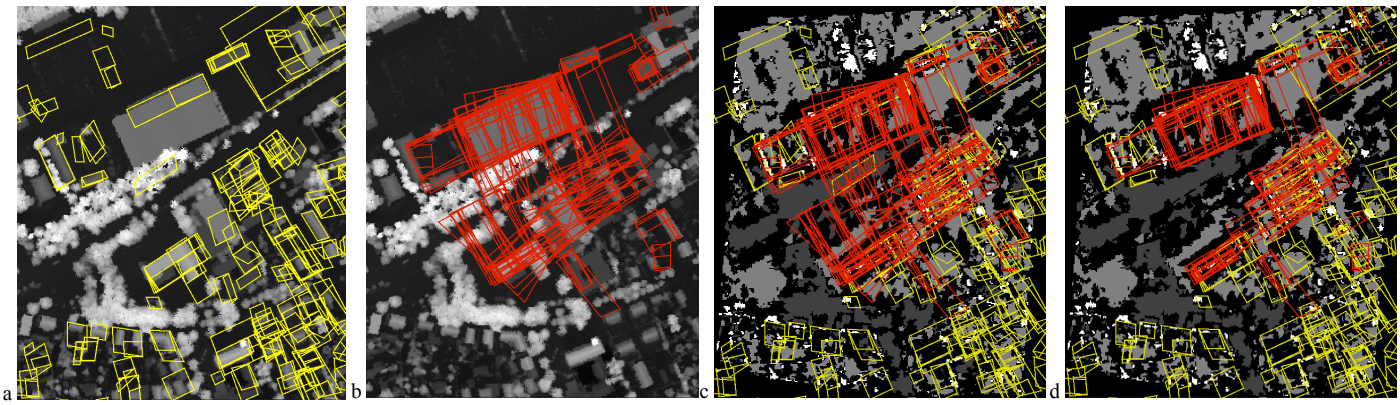

Figure 6. LIDAR DSM overlaid with assembled parallelograms (a) based on L-structures and generated quadrangles (b) based on Sensor-Close, Sensor-Far and Side edges; Classification result overlaid with assembled building hypotheses (c) and *Vegetation*-filtered building hypotheses(d)

IV. RESULTS

The developed approach was applied to an area of the test site Dorsten with a mixture of residential and industrial buildings. In Fig. 7a the reconstruction results are overlaid with an Orthophoto. The corresponding ground truth footprints taken from cadastral data are shown in Fig. 7b. The intersection result between the detected buildings and the cadastral ground truth data are depicted in Fig. 7c. The white areas represent the intersection of both. Light gray areas are part of the ground truth but were not detected, and dark gray marks areas which were detected in the SAR image but do not exist in the ground truth data (false positives).

Most of the extended buildings are well detected, because the considered SAR phenomena in the generation process were well observable and this group of buildings matches the underlying model in terms of form (prismatic object with a right-angled footprint). Most reconstructed footprints of the small buildings are larger compared to ground truth, such behavior was also reported in the literature [1]. In some cases layover of trees occluded corner lines, giving rise to a tendency of over-sized corner lines. Furthermore some of the small buildings are grouped close together in the ground truth data, which can lead to a common footprint in the detection result. Other small buildings were not detected because of too close proximity of neighbored buildings resulting in missing L-structures in the data.

For an assessment of the calculated InSAR heights inside the building polygons the LIDAR DSM is used as ground truth. The difference between ground truth and calculated height inside the intersection area (Fig. 7c) is shown in Fig. 7d. The above mentioned segmentation of too large footprints for smaller buildings reduced the mean InSAR height inside the detected footprints, because building heights as well as terrain heights contribute to the calculation. This effect and because some of the buildings have gabled roofs lead to higher height differences (lighter gray values) within small buildings (Fig. 7d). Furthermore, due to layover, the InSAR heights of small buildings are less reliable than the heights from extended ones.

Performance measures of the reconstruction results for the test site are characterized by a Detection Rate of 62% and a False Alarm Rate of 59%, which were calculated with the following formulas:

$$\text{Detection Rate} = \frac{\sum(\text{area}_{\text{cadastral}} \cap \text{area}_{\text{detected}})}{\sum(\text{area}_{\text{cadastral}})}$$

$$\text{False Alarm Rate} = \frac{\sum(\text{area}_{\text{detected}}) - \sum(\text{area}_{\text{cadastral}} \cap \text{area}_{\text{detected}})}{\sum(\text{area}_{\text{cadastral}})}$$

Furthermore for three buildings labeled in Fig. 7c the ground truth extension and height as well as the reconstruction results are given in Table I.

TABLE I. RECONSTRUCTION RESULTS

Building label	Ground truth data		Reconstruction result	
	size [m]	*height [m]*	*size [m]*	*height [m]*
A (extended)	100 x 53	85.9	106 x 60	86.4
B (residential)	17 x 11	86.5	19 x 16	84.2
C (church)	37 x 16	85.8 (103.8)	37 x 17	85.8

The size of the selected extended building (A) as well as the building height are well detected. The remaining differences are caused by a porch at the long side of the building. The footprint of the reconstructed small building (B) is too large as mentioned above. Following the mean height inside the polygon is estimated too low. Furthermore it is observable in the height differences (Fig. 7d), that the assumption of flat roof is wrong. The third building (C) marks a church. The footprint is well detected and the listed height results in Table I also let assume correctness, but the maximal height difference (+20 m) within the whole test site lies in this building footprint. This is caused by the spire of the church.

V. CONCLUSION

The presented approach is focused on the reconstruction of small as well as extended buildings, which are typical for mixed urban areas. A multi-aspect high resolution InSAR data set was investigated. Depending on the size and the relative

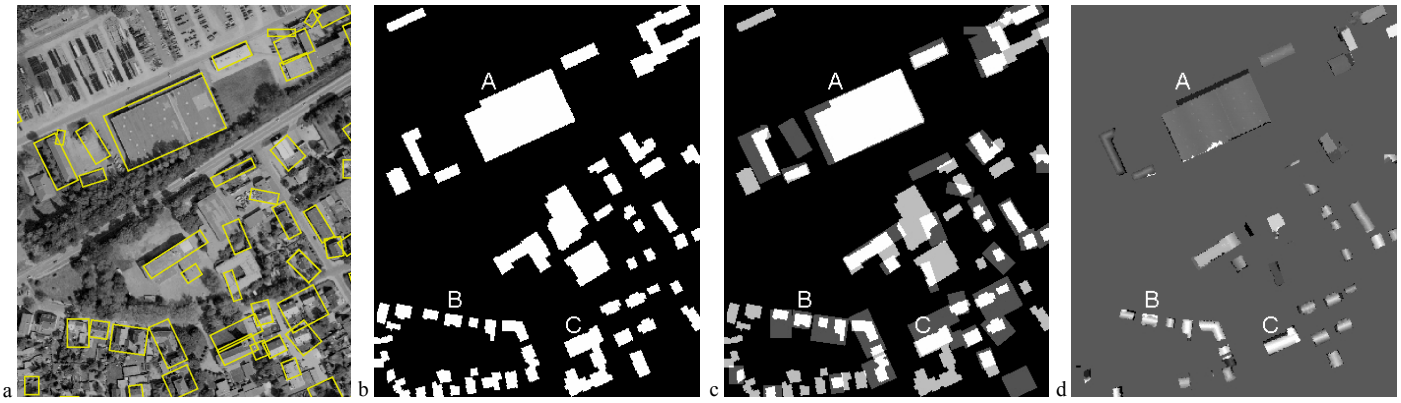

Figure 7. LIDAR DSM overlaid with final reconstruction results (a); Ground truth footprints (b); Overlay between the detection results and the ground truth footprints (c); Height difference between LIDAR DSM and interferometric heights at intersection area (d)

position of the building to the sensor, the considered SAR phenomena at building location for the detection and reconstruction were different.

The results achieved by the presented method shows the benefit of a combined analysis of small and extended building hints. This is advantageous especially in mixed urban areas, because no pre-classification into areas with residential respectively industrial character is necessary. A complete reconstruction of every building in the scene was not achieved. This is caused by a lack of segmented primitives at building locations, due to overlapping effects between neighbored buildings and trees, in this dense built-up area.

A topic of further investigation is the extension of the footprint shape to include more general right-angled outlines besides simple rectangular ones as considered here. Furthermore, an extension of the supported building models, for example outbuildings and gabled roofs, has to be integrated in an extended reconstruction approach.

REFERENCES

[1] P. Gamba, B. Houshmand, and M. Saccini, "Detection and Extraction of Buildings from Interferometric SAR Data," *IEEE Transactions on Geoscience and Remote Sensing*, vol. 38, no.1, 2000, pp. 611-618.

[2] R. Bolter, "Buildings from SAR: Detection and Reconstruction of Buildings from Multiple View High Resolution Interferometric SAR Data," Ph.D. dissertation, University Graz, 2001.

[3] U. Soergel, K. Schulz, and U. Thoennessen, "Phenomenology-based Segmentation of InSAR Data for Building Detection," in *Radig, B., Florczyk, S. (eds) Pattern Recognition*, 23rd DAGM Symposium, Springer, 2001, pp. 345-352.

[4] E. Simonetto, H. Oriot, and R.Garello, "Rectangular building extraction from stereoscopic airborne radar images," *IEEE Transactions on Geoscience and Remote Sensing*, vol. 43, no.10, 2005, pp. 2386-2395.

[5] J. H. G. Ender, and A. R. Brenner, "PAMIR - a wideband phased array SAR/MTI system," *IEE Proceedings - Radar, Sonar, Navigation*, vol. 150, no. 3, 2003, pp. 165-172.

[6] E. Michaelsen, U. Soergel, and U. Thoennessen, "Perceptual Grouping in Automatic Detection of Man-Made Structure in high resolution SAR data," *Pattern Recognition Letters, Special Issue Pattern Recognition in Remote Sensing,* vol. 27, no. 4, march 2006, pp. 218-225.

[7] U. Soergel, U. Thoenessen, A. Brenner, and U. Stilla, "High resolution SAR data: new opportunities and challenges for the analysis of urban areas", *IEE Proceedings - Radar, Sonar, Navigation*, 2006.

[8] U. Soergel, K. Schulz, U. Thoennessen, and U. Stilla, "Integration of 3D Data in SAR Mission Planning and Image Interpretation in Urban Areas". *Information Fusion, Elsevier B.V.*, vol. 6, no. 4, 2005, pp. 301-310.

[9] C. Tison, F. Tupin, J.-M. Nicolas, H. Maitre, "Validation of a feature fusion scheme for urban DSM retrieval from high resolution SAR interferogram". *Proc. IGARSS*, 2005, vol. 4, pp. 2795- 2798.

[10] D. G. Corr, A. Walker, U. Benz, I. Lingenfelder, A. Rodrigues, "Classification of urban SAR imagery using object oriented techniques," *Proc. IGARSS*, 2003, vol. 1, pp. 188-190.

[11] T. Esch, A. Roth, S. Dech, "Analysis of Urban Land Use Pattern Based on High Resolution Radar Imagery," *Proc. IGARSS*, 2006, CD Denver.

[12] G. Franceschetti, A. Iodice, and D. Riccio, "A canonical problem in electromagnetic backscattering from buildings," *IEEE Transactions on Geoscience and Remote Sensing*, vol. 40, 2002, pp. 1787-1801.

[13] T. Balz, "Automated CAD Model Based Geo-Referencing for High-Resolution SAR Data Fusion in Urban Environments", in *Proc. Of 5th European conference on synthetic aperture radar*, EUSAR 2004, pp. 427-430.

[14] M. Schwaebisch, and J. Moreira, "The high resolution airborne interferometric SAR AeS-1," *Proceedings of the Fourth International Air-borne Remote Sensing Conference and Exhibition*, Ottawa, Canada, 1999, pp. 540-547.

[15] A. Thiele, E. Cadario, K. Schulz, U. Thoennessen, and U. Soergel, "Building Recognition Fusing Multi-Aspect High-Resolution Interferometric SAR Data," *Proc. IGARSS*, 2006, CD ROM.

[16] A. Thiele, U. Thoennessen, E. Cadario, K. Schulz, and U. Soergel, "Building Recognition in Urban Areas from Multi-Aspect High-resolution Interferometric SAR Data," *Proc. EUSAR*, 2006, CD ROM.

[17] A. Lopes, E. Nezry, R. Touzi, and H. Laur, "Structure detection and statistical adaptive speckle filtering in SAR images", *International Journal of Remote Sensing,* vol. 14, no. 9, 1993, pp. 1735-1758.

[18] M. Borgeaud, U. Wegmueller, "On the Use of ERS SAR Interferometry for the Retrieval of Geo- and Bio-Physical Information", *FRINGE 96*, vol. 2, pp. 83-94.

[19] C. Steger, "An Unbiased Detector of Curvilinear Structures," *IEEE Transactions on Pattern Analysis and Machine Intelligence*, vol. 20, no. 2, 1986, pp. 113-125.

[20] J. Canny, "A Computational Approach to Edge Detection," *IEEE Transactions on Pattern Analysis and Machine Intelligence*, vol. 8, no. 6, 1986, pp. 679-698.

[21] U. Soergel, U. Thoennessen, and U. Stilla, "Iterative Building Reconstruction in Multi-Aspect InSAR Data," in *Maas HG, Vosselman G, Streilein A (eds) 3-D Reconstruction from Air-borne Laserscanner and InSAR Data, International Archives of Photogrammetry and Remote Sensing*, vol. 34, part 3/W13, 2003, pp. 186-192.